Journal of Magnetism and Magnetic Materials 551 (2022) 169133

Contents lists available at ScienceDirect

Journal of Magnetism and Magnetic Materials

journal homepage: www.elsevier.com/locate/jmmm

A comparative study of the magnetic and magnetocaloric effect of polycrystalline $Gd_{0.9}Y_{0.1}MnO_3$ and $Gd_{0.7}Y_{0.3}MnO_3$ compounds: Influence of Y-ions on the magnetic state of $GdMnO_3$

Afsar Ahmed [a], Dipak Mazumdar [a], Kalipada Das [b,*], I. Das [a]

[a] CMP Division, Saha Institute of Nuclear Physics, A CI of Homi Bhabha National Institute, 1/AF-Bidhannagar, Kolkata 700064, India
[b] Department of Physics, Seth Anandram Jaipuria College, 10-Raja Nabakrishna Stree, Kolkata 700005, India

ARTICLE INFO

Keywords:
Manganites
Magnetocaloric effect
Weak ferromagnetism
Relative cooling power

ABSTRACT

The modification of the magnetic ground state of the $GdMnO_3$ compound has been explored with Y-doping on the Gd-site. The study on the magnetic properties indicates the existence of a weak ferromagnetic phase upon a 10% Y-doped sample. However, the strength of the ferromagnetic interaction becomes feeble in the 30% Y-doped sample. Such modifications of the magnetic ground states are analyzed considering the breaking of correlated weak ferromagnetic chains due to doping of non-magnetic Y-ions. In addition to that, the magnetocaloric effect has also been affected by the doping concentrations of Y-ions. The significant value of magnetic entropy change and relative cooling power of both the studied systems indicate the possible utilization of the materials as efficient magnetic refrigerants at the cryogenic temperature.

1. Introduction

The suppression of the magnetic randomness in a magnetic material due to the influence of an external magnetic field, popularly known as the magnetocaloric effect (MCE) has been studied during the last few decades [1–7]. To elucidate the nature of magnetic ground state of any magnetic material, the MCE can be considered as a powerful tool [8–11]. It has been observed that a large value of MCE has appeared near the transition temperature regions (paramagnetic (PM)-ferromagnetic (FM)/antiferromagnetic (AFM) transition temperature). It is also considered as a more sensitive technique to detect any feeble magnetic transition as compared to the dc magnetization measurement technique [9,10]. Besides the fundamental importance, the MCE has also gained considerable attention from the technological perspective [12–14]. To substitute the vapor gas compression cooling procedure by magnetic refrigeration technique, the searching for new suitable refrigerant materials is one of the most quests to the current research direction [1,6]. It is important to find such refrigerant materials having working temperatures near room temperature or cryogenic temperature [2,3,8,15]. Due to the large magnetic moment of Gd-ions, the Gd-based compounds were extensively explored for several decades [12,16–29]. For the selection of a refrigerant material, the material should have large value of magnetic entropy change, moderate value of relative cooling power, good chemical stability, highly insulating, negligible thermal hysteresis, and the cost of material processing should be low. Considering those properties, the oxide-based materials have gained privileged attention over the intermetallic compounds [30–33]. In order to find out a suitable refrigerant material, a lot of research work has also been performed on undoped perovskite manganite ($AMnO_3$, A = trivalent ion) as well as doped perovskite manganite ($A_{1-x}B_xMnO_3$, A = trivalent ion, B = bivalent ion) compounds in the last twenty years [34–41].

Some of the well-studied undoped perovskite manganites are $LaMnO_3$, $GdMnO_3$, $YMnO_3$, etc. [30,31,34,42]. The $GdMnO_3$ compound exhibits rich magnetic properties due to its peculiar magnetic ground state configuration and temperature-induced phase transformation [34,43,44]. It is well documented that the $GdMnO_3$ shows a collinear sinusoidal incommensurate AFM phase, dominated by the Mn^{3+} spins at transition temperature, $T_N = 42$ K [34,45–48]. With further lowering the temperature, a canted A-type AFM phase has also appeared around T = 23 K [34,45–49]. However, the Gd^{3+} spins are antiferromagnetically coupled below T = 7 K [34]. Hemberger et al. had reported a detailed study about the magnetic ground state of the $GdMnO_3$ compound [45]. According to their study, a long-range order of Gd^{3+}-spins evolves at very low-temperature regions and results in a canting of the Gd^{3+} spins with a FM component [45]. This FM component is oriented anti-parallel to the FM moment that arises from the canted Mn^{3+}-spins [45].

* Corresponding author.
E-mail address: kalipadadasphysics@gmail.com (K. Das).

https://doi.org/10.1016/j.jmmm.2022.169133
Received 27 October 2021; Received in revised form 21 January 2022; Accepted 2 February 2022
Available online 12 February 2022

From the technical perspective, a refrigerant material should have a significant value of magnetic entropy change and negligible thermal hysteresis. The previous study indicates that the $GdMnO_3$ compound shows a significantly large MCE and hysteresis loop in the low-temperature regions [45]. The motivation of our present study is to explore the modification of the FM state by substitution of a non-magnetic Y^{3+} (Yttrium ion) on the Gd^{3+} site. Our experimental outcome indicates that due to the introduction of non-magnetic Y-ion, the hysteresis loop for weak FM interaction is substantially diminished as seen in the isothermal magnetization curves. Additionally, we have also observed significantly large values of magnetic entropy change and relative cooling power at the cryogenic temperature region for the Y^{3+}-doped $GdMnO_3$ compounds.

2. Experimental details

The polycrystalline compounds ($Gd_{1-x}Y_xMnO_3$; x = 0.1 and 0.3) were prepared by the well-known sol–gel method. At first, the appropriate amount of pre-heated rare earth oxide materials (Gd_2O_3 and Y_2O_3) and MnO_2 with high purity (99.99%) were taken. Both Gd_2O_3 and Y_2O_3 dissolved into millipore water, and then some amount of concentrated HNO_3 was added to make a clear solution. Due to the insoluble nature of MnO_2 in water as well as HNO_3, we have added the required amount of oxalic acid to make the manganese oxalate first and then added some HNO_3 to make it soluble in the solution. All the individual solutions were poured into a large beaker, and then the magnetic stirrer was used to make a homogeneous solution. After properly mixing up, a suitable amount of chelating agent such as citric acid was added and kept the solution undisturbed for some time. The solution was then uniformly heated at 80–90 °C using a water bath until the formation of a gel. The black porous powder was produced by heating the gel at 200–230 °C and the powder was burned at 500 °C for 4 h to remove any carbon component present in the system. Finally, the palletized form of the samples was annealed at 1300 °C for 36 h to achieve the bulk form of the compounds.

The room temperature X-ray diffraction (XRD) measurements had been carried out using a Rigaku-TTRAX-III diffractometer, from M/s Rigaku, Japan to characterize the compounds. The Cu-K_α source, having a wavelength of 1.5406 Å had been used for recording the XRD data at room temperature. To check the phase purity and to refine the unit cell parameters, the XRD data were refined (only profile fitted) by using the Rietveld refinement method in the Fullprof software. We had used the Pseudo-Voigt function and kept the scale factor as 1 during the whole refinement process. The magnetization measurements within the temperature range of 2–300 K and magnetic field variation up to ±70 kOe had been performed using a vibrating sample magnetometer-based superconducting quantum interference device (SQUID-VSM, Quantum Design, USA). The magnetization as a function of temperature at a particular magnetic field was measured using three different measurement protocols which are described as follows:

Zero-field-cooled-warming (ZFCW): The sample was first cooled down from room temperature to the lowest possible temperature without any external magnetic field. Then, the desired magnetic field was applied, and the magnetization data was recorded during the warming cycle.

Field-cooled-cooling (FCC): In the presence of the desired magnetic field, the temperature dependence of magnetization data was recorded during the cooling process from room temperature.

Field-cooled-warming (FCW): After the completion of the above mentioned FCC measurement, the sample was warmed from the low temperature to room temperature in presence of the same static magnetic field, and the corresponding magnetization data was collected.

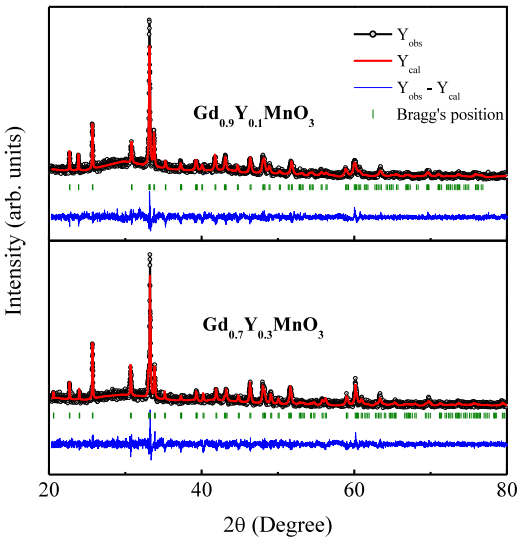

Fig. 1. Profile fitted XRD pattern of polycrystalline $Gd_{0.9}Y_{0.1}MnO_3$ and $Gd_{0.7}Y_{0.3}MnO_3$ compounds recorded at room temperature.

Table 1
Extracted lattice cell and refinement parameters of $Gd_{1-x}Y_xMnO_3$ (x = 0.1, 0.3) compounds.

Compound	a (Å)	b (Å)	c (Å)	V (Å^3)	R_{Bragg}	R_f	χ^2
$Gd_{0.9}Y_{0.1}MnO_3$	5.800(7)	7.455(8)	5.308(6)	229.453(9)	1.936	1.262	1.46
$Gd_{0.7}Y_{0.3}MnO_3$	5.820(3)	7.422(4)	5.294(3)	228.748(1)	2.631	1.590	1.45

3. Results and discussions

The room temperature XRD measurements indicate the single-phase nature of the compounds shown in Fig. 1. It is observed that both the compounds possess an orthorhombic crystal structure having a *Pnma* space group. The refined lattice cell parameters (a, b, c, and unit cell volume, V) and refinement factors (R_{Bragg}, R_f, and χ^2) for both the compounds are presented in Table 1.

A brief description regarding the ground state of the parent compound ($GdMnO_3$) should be discussed before the studied samples. A few debatable reports regarding the ground state of $GdMnO_3$ have been found in the literature [50,51]. In the context of effective ionic radius, this material lies on the boundary between A-type AFM and cycloid AFM phases [45,52]. In contrast to that Hemberger et al. had pointed out the non-spiral nature of the magnetic ground state in the absence of an external magnetic field [45]. This spiral nature of the magnetic ground state introduced a spontaneous polarization in the presence of a magnetic field [45,47].

In the present study, the magnetization as a function of temperature at H = 100 Oe external magnetic field for $Gd_{0.9}Y_{0.1}MnO_3$ and $Gd_{0.7}Y_{0.3}MnO_3$ compounds are presented in Fig. 2 (a) and (b) respectively. Similar to the $GdMnO_3$, the $Gd_{0.9}Y_{0.1}MnO_3$ sample transforms from a PM state to an incommensurate AFM state near T = 42 K. This incommensurate AFM phase is dominated by Mn^{3+} ions, which are aligned opposite to the direction of the applied magnetic field. With further decreasing the temperature, the PM Gd^{3+} ions are started to align along the applied field direction [45]. The competitive AFM magnetization arising from the Gd^{3+} and Mn^{3+} spins increases down to 7 K. At the very low-temperature region (T < 7 K), the ZFCW magnetization data indicates a decreasing nature due to the AFM ordering of neighboring Gd^{3+} spins [34,45]. On the other hand, such AFM signature is hindered in the FCC/FCW magnetization data. The FC magnetization increases monotonically with lowering the temperature. However, for the $Gd_{0.7}Y_{0.3}MnO_3$, the temperature dependence of magnetization curves follows the identical nature with a small kink at the

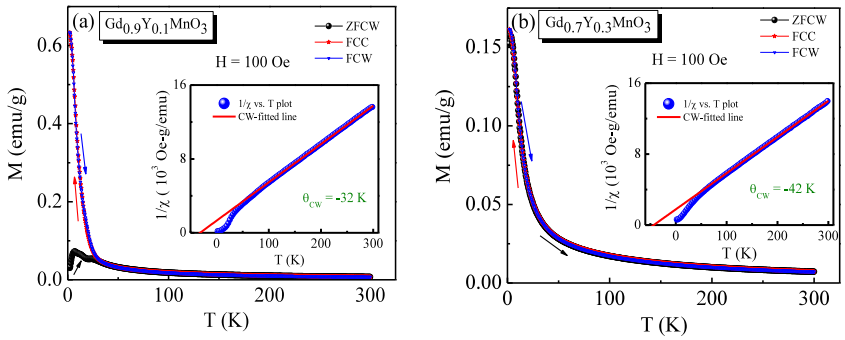

Fig. 2. Variation of magnetization with temperature at H = 100 Oe in three different measurement protocols ZFCW, FCC and FCW for (a) $Gd_{0.9}Y_{0.1}MnO_3$ and (b) $Gd_{0.7}Y_{0.3}MnO_3$ compounds. Insets show the variation of inverse susceptibility ($1/\chi$) with temperature for both the compounds.

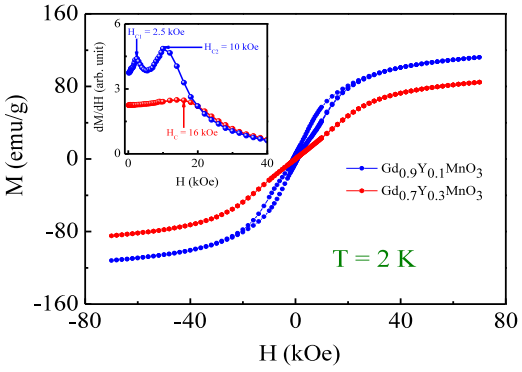

Fig. 3. Isothermal magnetization curve as a function of external magnetic field at T = 2 K. Blue data points shows the hysteresis for $Gd_{0.9}Y_{0.1}MnO_3$ compound and red data points shows no such hysteresis for $Gd_{0.7}Y_{0.3}MnO_3$ compound. Inset shows the dM/dH vs. H plots for both the compounds.

very low-temperature region. This suggests the existence of a dominant AFM transition.

For a better understanding of the magnetic ground state, we have plotted the inverse susceptibility ($1/\chi$) as a function of temperature for both the compounds as shown in the respected insets of Fig. 2 (a) and (b). We have fitted the $1/\chi$ vs. T plots using the Curie–Weiss law (CW) of the form $\chi = C/(T - \theta_{CW})$ (where C is the Curie constant). The estimated values of Curie–Weiss temperature, θ_{CW} are −32 K and −42 K for $Gd_{0.9}Y_{0.1}MnO_3$ and $Gd_{0.7}Y_{0.3}MnO_3$ compounds respectively. The negative value of θ_{CW} for both the compounds suggests the dominating nature of the AFM ground states.

To get a deeper view of the magnetic ground state, we have measured the magnetization as a function of magnetic field at T = 2 K for both the compounds as shown in Fig. 3. With increasing the magnetic field, a noticeable change in magnetization data has been observed in the studied compounds. The isothermal magnetization data indicates the predominant field-induced FM phase for both compounds. In the first derivative of magnetization data (dM/dH vs. H) as shown in the inset of Fig. 3, we have observed prominent peaks for both the compounds. The peak positions are corresponding to the critical field values (H_C) for meta-magnetic-type phase transition. This suggests the presence of mixed magnetic phases (AFM+FM) in the studied systems at low temperature regions. Additionally, the $Gd_{0.9}Y_{0.1}MnO_3$ sample exhibits a pronounced hysteresis loop. However, such hysteresis nature is absent in the case of $Gd_{0.7}Y_{0.3}MnO_3$ compound. As the doping concentration of non-magnetic Y^{3+} ions increases, the FM correlation between Y^{3+} and Gd^{3+} ions becomes weaker in the presence of the magnetic field. This can be observed in the M–H curves (Fig. 3) where no such prominent hysteresis loop is present for the $Gd_{0.7}Y_{0.3}MnO_3$ system. The reversible nature of the magnetization implies the minimization of magnetic energy loss. Regarding this context, the presence of magnetic field hysteresis in the M–H curves and the absence of thermal hysteresis in the M–T curves should be a beneficial aspect for the selection of any magnetic refrigerant materials.

According to the earlier report, a significantly large value of magnetic entropy change has been observed in the single-crystalline $GdMnO_3$ compound [34]. For evaluating the magnetocaloric performance of the compounds, we have carried out the isothermal magnetization measurements at several fixed temperatures. Some of the selected magnetic isotherms are shown in Fig. 4 (a) and (b) for both the compounds. The M^2 vs. H/M curves (Arrott plot) from 2 K to 24 K with a temperature difference of 2 K have also been plotted in Fig. 4. In Fig. 4 (c) and (d), the positive slopes of the Arrott plots indicate the second order nature of the magnetic phase transition for both the compounds.

The magnetic entropy change (ΔS_m) has been calculated using Maxwell's thermodynamics relation, which is given below:

$$\Delta S_m = \int_0^H (\partial M/\partial T) dH \quad (1)$$

The magnetic entropy change is directly related to the change in magnetization of the sample with the temperature. Hence, a large value of ΔS_m should be expected only at the low-temperature region for the present systems (Fig. 2). The estimated $-\Delta S_m$ as a function of temperature for $Gd_{0.9}Y_{0.1}MnO_3$ and $Gd_{0.7}Y_{0.3}MnO_3$ compounds have been shown in Fig. 5 (a) and (b) respectively. The temperature dependent $-\Delta S_m$ exhibits a quietly large value at the cryogenic temperature region. Due to the presence of a strong AFM ground state in the $Gd_{0.9}Y_{0.1}MnO_3$ system, the $-\Delta S_m$ vs. T curves show an inverse MCE at T = 3 K for a field change of 10 kOe as shown in Fig. 5 (a).

In addition to the large value of $-\Delta S_m$, the value of relative cooling power (RCP) is also important for any refrigerant material. RCP simply depends on the maximum value of $-\Delta S_m$ and its temperature broadening. The value of RCP can be estimated by using the expression, RCP = $|-\Delta S_m^{max}| \times \Delta T_{FWHM}$, where $-\Delta S_m^{max}$ is the maximum value of magnetic entropy change at a constant applied field value and ΔT_{FWHM} is the full-width at half-maxima of $-\Delta S_m$ vs. T curves. The variation of RCP as a function of magnetic fields for $Gd_{0.9}Y_{0.1}MnO_3$ and $Gd_{0.7}Y_{0.3}MnO_3$ compounds have been presented in Fig. 5 (c) and (d) respectively. For $Gd_{0.9}Y_{0.1}MnO_3$, the maximum value of RCP is 390 J/kg, and the corresponding value of $-\Delta S_m^{max}$ is 22.65 J/(kg K) upon a field change of 70 kOe. For the $Gd_{0.7}Y_{0.3}MnO_3$ compound, the maximum value of RCP is 262 J/kg, and the corresponding value of $-\Delta S_m^{max}$ is 15 J/(kg K) for ΔH = 70 kOe. In addition to the large value of $-\Delta S_m^{max}$, both the compounds exhibit significantly large values of RCP at the cryogenic temperature region. Regarding this issue, we have compared these maximum values of magnetic entropy change ($-\Delta S_m^{max}$) and RCP at the low-temperature region with several other manganite compounds in Table 2. In contrast to the single-crystalline $GdMnO_3$, the magnetic anisotropy is highly influenced the magnetocaloric properties for the polycrystalline form of the compound [53]. As reported by Mahana et al. the maximum

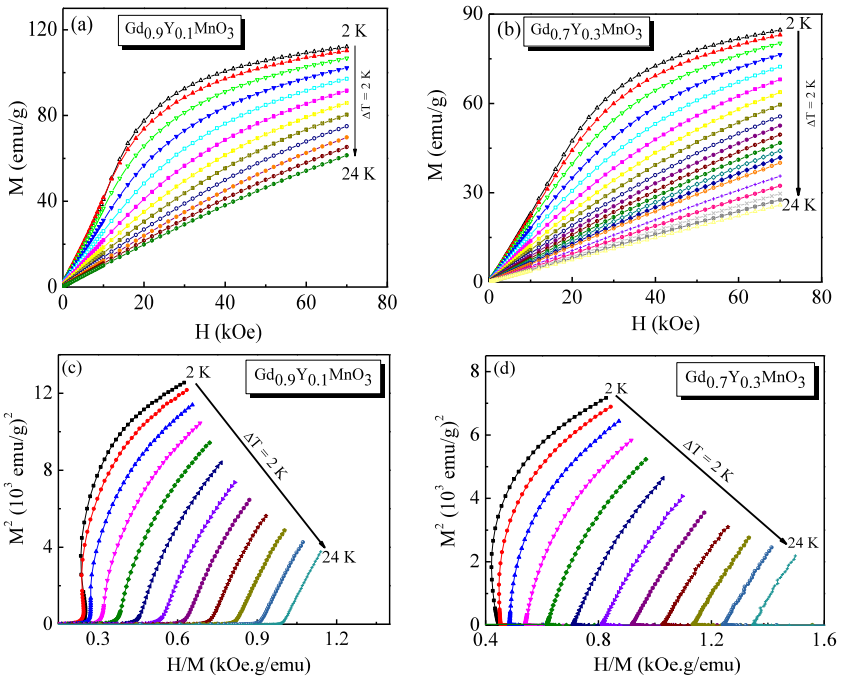

Fig. 4. Isothermal magnetization as a function of external magnetic field at several fixed temperatures for polycrystalline (a) $Gd_{0.9}Y_{0.1}MnO_3$ and (b) $Gd_{0.7}Y_{0.3}MnO_3$ compounds. (c) and (d) represent the Arrott plots (M^2 vs. H/M) of the $Gd_{0.9}Y_{0.1}MnO_3$ and $Gd_{0.7}Y_{0.3}MnO_3$ compounds respectively.

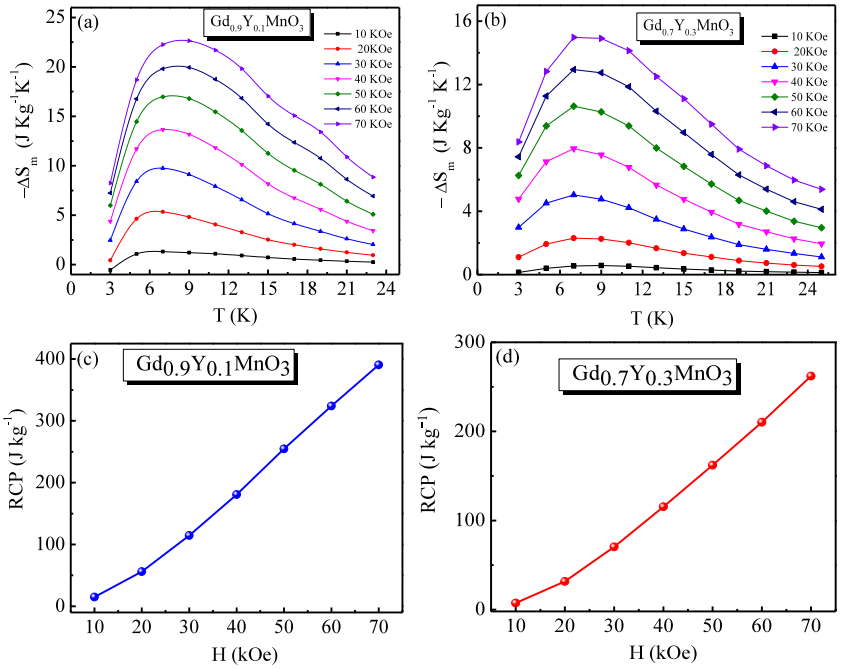

Fig. 5. Magnetocaloric effect: Magnetic entropy change ($-\Delta S_m$) vs. temperature at different external magnetic fields for (a) $Gd_{0.9}Y_{0.1}MnO_3$ and (b) $Gd_{0.7}Y_{0.3}MnO_3$ compounds. (c) and (d) represent the variation of relative cooling power (RCP) as a function of external magnetic field for both the compounds.

value of the magnetic entropy change ($-\Delta S_m^{max}$) is reduced in the case of polycrystalline form of the sample [53]. In our present study, the value of magnetic entropy change for $Gd_{0.9}Y_{0.1}MnO_3$ compound is higher and the same is comparable to the parent polycrystalline $GdMnO_3$ compound in case of the $Gd_{0.7}Y_{0.3}MnO_3$ compound [53]. Moreover, the RCP values of both Y-doped compounds are higher than the polycrystalline $GdMnO_3$ compound [53].

Additionally, the $-\Delta S_m$ vs. T curves of $Gd_{0.9}Y_{0.1}MnO_3$ and $Gd_{0.7}Y_{0.3}MnO_3$ compounds can also be understood using a universal master entropy change curve [54,55]. For the second-order magnetic phase transition, the universal master curve is constructed by normalizing the magnetic entropy change with their respective maximum value ΔS_m^{max} and rescaling the temperature axis as θ which is defined by

$$\theta = -\frac{(T - T_c)}{(T_{r1} - T_c)} \ldots\ldots\ldots T \le T_c \quad (2)$$

$$\theta = \frac{(T - T_c)}{(T_{r2} - T_c)} \ldots\ldots\ldots T > T_c \quad (3)$$

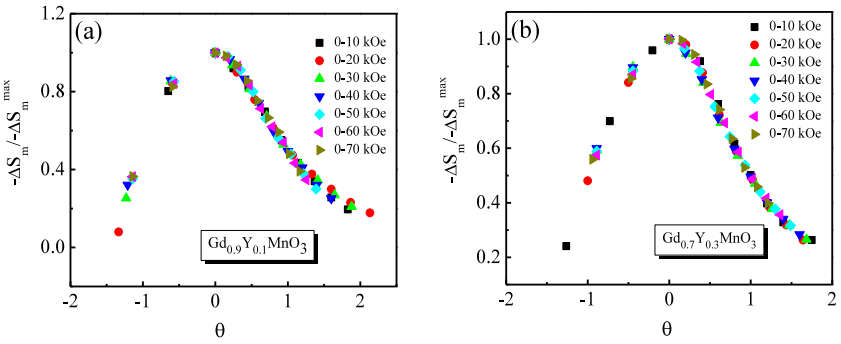

Fig. 6. Variation of the normalized magnetic entropy change with reduced temperature for (a) $Gd_{0.9}Y_{0.1}MnO_3$ and (b) $Gd_{0.7}Y_{0.3}MnO_3$ compounds.

Table 2
Comparison of magnetocaloric parameters ($-\Delta S_m^{max}$ and RCP) of several manganite compounds at low temperature region.

Compound	H (kOe)	$-\Delta S_m^{max}$ (J/kg-K)	RCP (J/kg)	References
$Gd_{0.9}Y_{0.1}MnO_3$	70	22.65	390	Present study
$Gd_{0.7}Y_{0.3}MnO_3$	70	15.0	262	Present study
$GdMnO_3$ (c axis)	70	29.76	420	[34]
$GdMnO_3$ (a axis)	70	23.55	285	[34]
$GdMnO_3$ (polycrystal)	70	15.43	211	[53]
$ErMnO_3$	30	9.4	–	[41]
$Gd_{0.5}Ca_{0.5}MnO_3$	70	22.8	–	[35]
$Dy_{0.5}Ca_{0.5}MnO_3$	70	8.5	–	[35]
$Dy_{0.5}Sr_{0.5}MnO_3$	50	4.0	144	[38]
$Dy_{0.5}(Sr_{0.9}Ca_{0.1})_{0.5}MnO_3$	50	2.5	113	[38]
$Dy_{0.5}(Sr_{0.7}Ca_{0.3})_{0.5}MnO_3$	50	5.0	169	[38]
$La_{0.8}Ca_{0.2}Mn_{0.8}Fe_{0.2}O_3$	50	0.54	–	[39]
Gd_2CoMnO_6	90	25.4	–	[40]

where T_{r1} and T_{r2} are the reference temperatures of each $-\Delta S_m$ vs. T curve corresponding to half of the maximum entropy change value. The variation of the normalized entropy change curve with θ of $Gd_{0.9}Y_{0.1}MnO_3$ and $Gd_{0.7}Y_{0.3}MnO_3$ compounds are shown in Fig. 6 (a) and (b) respectively. It has been noticed that all the rescaled normalized entropy change curves (for different magnetic field values) are collapsed into one single master curve for both the compounds. This confirms the occurrence of the second-order magnetic phase transition at around 7 K [15]. Additionally, absence of reasonable deviation in the universal curves indicates the absence of spin reorientation phenomenon or spin-glass transition in the present studied compounds [15].

For the $Gd_{0.9}Y_{0.1}MnO_3$ compound, all the three magnetization measurement protocols show a similar trend at T > 42 K, but the ZFCW magnetization curve does not follow the same track unlike the FCC or FCW magnetization data below T < 42 K. A phase transformation of Mn^{3+} ion takes place from the PM state to an incommensurate AFM state at T = 42 K for the parent $GdMnO_3$ compound [34]. Due to the absence of spontaneous magnetization, a drastic change in magnetization has not been observed in the parent compound [34]. With further decreasing temperature, the ground states of Gd^{3+} sublattices are coupled ferromagnetically with each other in the absence of any magnetic field. At the same time, the strength of canting component of Mn^{3+} ions is small which results in a weak FM behavior at the very low-temperature region. The clear evidence of this weak FM state is shown in Fig. 3 as field hysteresis is present at the low temperature. However, the scenario is completely different in the case of FCC and FCW magnetization data as compared to the ZFCW magnetization data. In the presence of an external magnetic field, all the Gd^{3+} spins are oriented parallel to the applied magnetic field direction and the resultant magnetization increases with decreasing temperature due to the large magnetic moment of Gd^{3+} ions as compared to the resultant magnetic moment of the canted Mn^{3+} ions. The presence of weak ferromagnetic behavior in the studied systems can also be understood with the doped non-magnetic Y^{3+}-ions. As the Gd^{3+} (ionic radius is 1.107 Å) ions are replaced by comparatively lower ionic radii-based cations such as Y^{3+}-ions (ionic radius is 1.075 Å), the unit cell parameters and volume decrease. The Mn–O–Mn bond angle and Mn–O bond lengths are also reduced with the substitution of Y^{3+}-ions [56]. When the doping concentration of the non-magnetic Y^{3+} is 10%, the correlation among the Gd^{3+}-ions becomes weak. Due to the reduction of Mn–O–Mn bond angle, the resultant magnetic moment of the canted Mn^{3+}-ions increases which reduces the width of the FM hysteresis loop. This feature is totally absent in the higher Y^{3+}-doped compound (x = 30%). In the case of virgin compound, each magnetic Gd^{3+}-ion is coupled with the neighboring Gd^{3+}-ions and shows a weak FM state. As the doping concentration of non-magnetic Y^{3+}-ions increases, the magnetic correlation becomes weak and the weak FM phase diminishes.

4. Conclusions

In summary, the magnetic and magnetocaloric properties of $Gd_{0.9}Y_{0.1}MnO_3$ and $Gd_{0.7}Y_{0.3}$ MnO_3 compounds have been presented in details. As a result of Y-doping on the Gd-site, the magnetic ground state of the parent material ($GdMnO_3$) is markedly modified. Additionally, the long-range FM interaction strength is suppressed with the doping of Y^{3+}-ion. For the 30% Y-doped sample, the FM hysteresis loop in magnetization is totally disappeared. At the cryogenic temperature, due to the large values of magnetic entropy change and other beneficial aspects (insulating nature, high chemical stability, large RCP, small or no thermal hysteresis), both the compounds can be considered as promising magnetic refrigerant materials.

Declaration of competing interest

The authors declare that they have no known competing financial interests or personal relationships that could have appeared to influence the work reported in this paper.

Data availability:

The data that support the findings of this study are available from the corresponding author upon reasonable request.

Acknowledgment

The work was supported by Department of Atomic Energy (DAE), Govt. of India.

References

[1] A. Kitanovski, J. Tusek, U. Tomc, U. Plaznik, M. Ozbolt, A. Poredos, Magnetocaloric Energy Conversion: From Theory to Applications, Springer International Publishing, Cham, 2015.
[2] X.Y. Zhang, Y. Chen, Z.Y. Li, J. Phys. D: Appl. Phys. 40 (2007) 3243.
[3] K. Das, S. Banik, I. Das, Mater. Res. Bull. 73 (2016) 256.
[4] A.O. Pecharsky, K.A. Gschneidner Jr., V.K. Pecharsky, J. Appl. Phys. 93 (2003) 4722.
[5] F. Canepaa, M. Napoletano, S. Cirafici, Intermetallics 10 (2002) 731.
[6] N.A. de Oliveira, P.J. von Ranke, Phys. Rep. 489 (2010) 89.
[7] H. Wada, Y. Tanabe, Appl. Phys. Lett. 79 (2001) 3302.
[8] T. Samanta, I. Das, S. Banerjee, J. Appl. Phys. 104 (2008) 123901.
[9] K. Das, N. Banu, I. Das, B.N. Dev, J. Magn. Magn. Mater. 487 (2019) 165309.
[10] A. Biswas, T. Samanta, S. Banerjee, I. Das, Appl. Phys. Lett. 94 (23) (2009) 233109.
[11] D. Mazumdar, K. Das, S. Roy, I. Das, J. Magn. Magn. Mater. 497 (2020) 166066.
[12] K.A. Gschneidner Jr., V.K. Pecharsky, A.O. Tsokol, Rep. Progr. Phys. 68 (2005) 1479.
[13] A.M. Tishin, Y.I. Spichkin, The Magnetocaloric Effect and its Applications, Institute of Physics Publishing, Bristol and Philadelphia, 2003.
[14] A.M. Tishin, Magnetic therapy of malignantneoplasms by injecting material particles with high magnetocaloritic effect and suitable magnetic phase transition temperature, 2008, Patent number:EP1897590-A1.
[15] Y. Zhang, Y. Yang, X. Xu, S. Geng, L. Hou, X. Li, Z. Ren, G. Wilde, Sci. Rep. 6 (2016) 34192.
[16] V.K. Pecharsky, K.A. Gschneidner Jr., Phys. Rev. Lett. 78 (1997) 4494.
[17] V.K. Pecharsky, K.A. Gschneidner Jr., J. Magn. Magn. Mater. 167 (1997) L179.
[18] V.K. Pecharsky, K.A. Gschneidner Jr., J. Alloys Compd. 260 (1997) 98.
[19] V.K. Pecharsky, K.A. Gschneidner Jr., Appl. Phys. Lett. 70 (1997) 3299.
[20] V. Provenzano, A.J. Shapiro, R.D. Shull, Nature 429 (2004) 853.
[21] R.D. Shull, V. Provenzano, A.J. Shapiro, A. Fu, M.W. Lufaso, J. Karapetrova, G. Kletetschka, V. Mikula, J. Appl. Phys. 99 (2006) 08k908.
[22] J.Q. Li, W.A. Sun, Y.X. Jian, Y.H. Zhuang, W.D. Huang, J.K. Liang, J. Appl. Phys. 100 (2006) 073904.
[23] Y.H. Zhuang, J.Q. Li, W.D. Huang, W.A. Sun, W.Q. Ao, J. Alloys Compd. 421 (2009) 49.
[24] D.M.R. Kumar, M.M. Raja, R. Gopalan, A.S. Rao, V. Chandrasekaran, J. Magn. Magn. Mater. 321 (2009) 1300.
[25] F. Casanova, X. Batlle, A. Labarta, J. Marcos, L. Manosa, A. Planes, Phys. Rev. B 66 (2002) 212402.
[26] C. Magen, Z. Arnold, L. Morellon, Y. Skorokhod, P.A. Algarabel, M.R. Ibarra, J. Kamarad, Phys. Rev. Lett. 91 (2003) 207202.
[27] W. Choe, V.K. Pecharsky, A.O. Pecharsky, K.A. Gschneidner Jr., V.G. Young Jr., G.J. Miller, Phys. Rev. Lett. 84 (2000) 4617.
[28] R. Mondal, R. Nirmala, J.A. Chelvane, A.K. Nigam, J. Appl. Phys. 113 (2013) 17A930.
[29] R. Nirmala, A.V. Morzkin, S.K. Malik, J. Phys. 84 (6) (2015) 977.
[30] A. Jabar, R. Masrour, Phase Transit. 91 (3) (2017) 284.
[31] A. Biswas, S. Chandra, M.H. Phan, H. Srikanth, J. Alloys Compd. 545 (2012) 157.
[32] K.P. Shinde, V.M. Tien, L. Huang, H.R. Park, S.C. Yu, K.C. Chung, D.H. Kim, J. Appl. Phys. 127 (2020) 054903.
[33] A. Barman, S.K. Narayan, D. Mukherjee, Adv. Mater. Interfaces 6 (2019) 190029.
[34] A.A. Wagh, K.G. Suresh, P.S.A. Kumar, S. Elizabeth, J. Phys. D: Appl. Phys. 48 (2015) 135001.
[35] K. Das, T. Paramanik, I. Das, J. Magn. Magn. Mater. 374 (2015) 707.
[36] T. Tang, K.M. Gu, Q.Q. Cao, D.H. Wang, S.Y. Zhang, Y.W. Du, J. Magn. Magn. Mater. 222 (2000) 110.
[37] A.M. Gomes, M.S. Reis, A.P. Guimaraes, P.B. Tavares, J.P. Araujo, V.S. Amaral, J. Magn. Magn. Mater. 2385 (2004) 272.
[38] R. Hamdi, A. Tozri, M. Smari, E. Dhahri, L. Bessais, Chem. Phys. Lett. 680 (2017) 94.
[39] D. Fatnassi, K. Sbissi, E.K. Hlil, M. Ellouze, J.L. Rehspringer, F. Elhalouani, J. Nanostruct. Chem. 5 (2015) 375.
[40] J.Y. Moon, M.K. Kim, Y.J. Choi, N. Lee, Sci. Rep. 7 (2017) 16099.
[41] K. Das, S. Banik, I. Das, Phys. B 533 (2018) 46.
[42] S. Chandra, A. Biswas, S. Datta, B. Ghosh, V. Siruguri, A.K. Raychaudhuri, M.H. Phan, H. Srikanth, J. Phys. Condens. Matter 24 (2012) 366004.
[43] P. Negi, G. Dixit, H.M. Agrawal, R.C. Srivastava, J. Supercond. Nov. Magn. 26 (5) (2012) 1611.
[44] X.L. Wang, D. Li, T.Y. Cui, P. Kharel, W. Liu, Z.D. Zhang, J. Appl. Phys. 107 (2010) 09B510.
[45] J. Hemberger, S. Lobina, H.A.K. von Nidda, N. Tristan, V.Y. Ivanov, A.A. Mukhin, A.M. Balbashov, A. Loidl, Phys. Rev. B 70 (2004) 024414.
[46] R. Vilarinho, A. Almeida, J.M.M. da Silva, J.B. Oliveira, M.A. Sa, P.B. Tavares, J.A. Moreira, Solid State Commun. 208 (2015) 34.
[47] T. Kimura, G. Lawes, T. Goto, Y. Tokura, A. Ramirez, Phys. Rev. B 71 (2005) 224425.
[48] T. Arima, T. Goto, Y. Yamasaki, S. Miyasaka, K. Ishii, M. Tsubota, T. Inami, Y. Murakami, Y. Tokura, Phys. Rev. B 72 (2005) 100102.
[49] T. Goto, Y. Yamasaki, H. Watanabe, T. Kimura, Y. Tokura, Phys. Rev. B 72 (2005) 220403.
[50] J. Baier, D. Meier, K. Berggold, J. Hemberger, A. Balbashov, J.A. Mydosh, T. Lorenz, Phys. Rev. B 73 (2006) 100402(R).
[51] H. Kuwahara, M. Akaki, J. Tozawa, M. Hitomi, K. Noda, D. Akahoshi, J. Phys.: Conf. Ser. 150 (2009) 042106.
[52] M. Mochizuki, N. Furukawa, Phys. Rev. B 80 (2009) 134416.
[53] S. Mahana, U. Manju, D. Topwal, J. Phys. D: Appl. Phys. 50 (2017) 035002.
[54] V. Franco, A. Conde, J.S. Blazquez, Appl. Phys. Lett. 89 (2006) 222512.
[55] V. Franco, A. Conde, J.M. Romero-Enrique, J.S. Blazquez, J. Phys.: Condens. Matter 20 (2008) 285207.
[56] R.M. Sarguna, V. Sridharan, S. Shanmukrao, V. Ganesan, S. Bhardwaj, A.M. Awasthi, M.D. Mukadam, S.M. Yusuf, A.K. Sinha, N. Subramanian, J. Phys.: Condens. Matter 26 (2014) 345901.